arXiv:1002.2843v1 [physics.chem-ph] 15 Feb 2010

Decoherence in Weakly Coupled Excitonic Complexes

Tomáš Mančal[1], Vytautas Balevičius Jr.[1,2], and Leonas Valkunas[2,3]
[1] *Charles University in Prague, Faculty of Mathematics and Physics, Ke Karlovu 5, CZ-121 16 Prague 2, Czech Republic,*
[2] *Department of Theoretical Physics, Faculty of Physics of Vilnius University, Sauletekio Avenue 9, build. 3, LV-10222 Vilnius and* [3] *Institute of Physics, Savanoriu Avenue 231, LV-02300 Vilnus, Lithuania*

Equations of motion for weakly coupled excitonic complexes are derived. The description allows to treat the system in the basis of electronic states localized on individual chromophores, while at the same time accounting for experimentally observable delocalization effects in optical spectra. The equations are show to be related to the well-known Förster type energy transfer rate equations, but unlike Förster equations, they provide a description of the decoherence processes leading to suppression of the resonance coupling by bath fluctuations. Linear absorption and two-dimensional photon echo correlation spectra are calculated for simple model systems in homogeneous limit demonstrating distinct delocalization effect and reduction of the resonance coupling due to interaction with the bath.

I. INTRODUCTION

Excitonic interaction determines spectroscopic and functional properties of many naturally occurring, as well as artificially synthesized macromolecular systems [1–5]. The great variability of photosynthetic antennae of plants and bacteria that involve only a limited number of different types of small molecules as building blocks, is to a high degree enabled by the large influence of interchromophore interactions on spectral and energy transfer properties of closely packed protein-chromophore complexes [3, 6]. In recent years, some of the properties and function of photosynthetic antennae were linked both theoretically [7, 8] and experimentally [9–11] to various types of coherence effects. In some photosynthetic complexes, dynamics related to long-lasting electronic coherences was observed during relaxation of excitation energy at 77 K and even at room temperature [9, 12], and it was speculated that the coherent mode of energy transfer can improve the robustness of the energy transfer process [9, 13]. While quantitative aspect of this improvement is a matter of ongoing research, another closely related type of coherence, the one accompanying delocalization of excited states in weakly coupled chromophore complexes, has been found to play a significant role in spectra and energy relaxation rates of some bacterial antenae. For the peripheral bacterial light harvesting complexes LH2 and LH3, it has been shown that event at very weak resonance coupling the absorption spectra, relaxation rates and coherent two-dimensional electronic spectra show characteristic features of delocalization [7, 14].

Proteins fix the positions of chromophores in a protein-chromophore complex, and thus determine their mutual interactions. However, the protein surrounding also tune local excitation energies of the chromophores to achieve further flexibility of the antennae [15]. The protein environment influences the electronic degrees of freedom (DOF) also on the ultrafast time scale. The shape of the absorption line of a separate molecule is defined by the interaction of electronic transition with the intramolecular vibrations and vibrations (phonons) of a molecular surrounding. The concept of line-shape function originates from pioneering theoretical work by Lax on absorption spectrum of a two-level system coupled to harmonic oscillators [16]. Further development of the theory has been based on the stochastic approach [17, 18], description of anharmonicity [19] and the Brownian oscillator model for the phonon system [20]. In molecular aggregates the intermolecular interactions compete with the electronic transition coupling to the intramolecular vibrations and phonons, which both are usually considered as thermal bath fluctuations.

Two-limiting cases of relative strength of the resonance interaction and the electron-phonon coupling are widely used in various theoretical methods. In the strong exciton coupling regime (with respect to electron phonon interaction) the homogeneous bandwidths of the absorption/emission spectra and spectral dynamics are related to the exciton relaxation (dephasing) caused by the thermal bath fluctuations. Excitonic splitting of the transition energies due to the resonance interaction schematically illustrated in Fig. 1, dominates absorption spectrum. In the opposite regime, the intermolecular resonance interaction might be considered perturbatively. The excitation dynamics is then characterized by hopping between the chromophore molecules, and can be well described by the Förster theory. Förster resonance energy transfer (FRET) is nowadays widely accepted as a molecular ruler in various biological systems [21, 22].

The above mentioned photosynthetic complex LH2 is a good example of a system where both these limiting cases persist. This complex is arranged as a highly symmetric ring of 9 (or 8 depending on the species of bacteria) protein-chromophore subunits, each containing two helical trans-membrane polypeptides, the α-polypeptide on the inner side and the β-polypeptide on the outer side of the ring [3]. The carboxy-terminal domain of this protein binds, in the hydrophobic membrane phase, a ring of 18 (or 16 depending on the species of bacteria) tightly coupled bacteriochlorophyll (Bchl) molecules with a center-

to-center distance of less than 1 nm between neighboring chromophores. This ring is responsible for the intense absorption of LH2 at 850 nm (the so called B850 ring). Due to the relatively small distances between the chromophores in the B850 ring the interaction between Bchl molecules plays an important role in determining their spectroscopic and functional properties. A second ring of 9 (or 8) weakly interacting Bchls is bound by the amino-terminal domain of LH2 (chromophore-chromophore distance of about 2.1 nm) and is largely responsible for the absorption at 800 nm (the B800 ring). Most of the spectroscopic results for B850 band can be well explained in terms of the exciton model invoking available structural data [23, 24]. However, the single molecular fluorescence data and studies of the temperature dependence of the absorption spectra reveal that the conventional exciton model has to be modified due to the exciton interaction with the protein surrounding. The modified (dichotomous) exciton model was proposed to explain these discrepancies [25–27]. In contrast, the absorption and excitation dynamics in the B800 ring are usually considered in terms of localized excitations of individual chromophores, due to the weakness of the intermolecular coupling. Despite of that, signatures of weak excitonic coupling have also been identified in the optical spectra of photosynthetic antennae of LH2 [7], single molecular excitation spectra at low temperatures [28], and 2D spectra of its analogous LH3 complex [14]. Similar effects can be expected in other molecular aggregates with weakly coupled chromophores, DNA stacks, polymers, etc.

In this paper we formulate and develop a theoretical model, which allows us to describe exciton dynamics in the system of weakly coupled molecular aggregates in terms of the reduced density matrix (RDM) in the basis of the site representation of the chromophores. The exciton coupling is treated as a perturbation and equations of motion (EM) for the RDM are derived in the second order. This enables us to retain main excitonic effects such as transition dipole moment redistribution, transition energy shift and a characteristic excited state absorption (ESA) shift, while simultaneously working with localized states.

The paper is organized as follows. In the next section, we introduce the model system and its Hamiltonian. In Section III we derive EM for a general weakly coupled excitonic complex, and in Section IV we discuss long time limit of these equations, leading to Förster type of relaxation. We discuss calculations of linear absorption and two-dimensional photo-echo spectra in Section V. Model calculations are presented in Section VI.

II. MODEL HAMILTONIAN

Let us consider an aggregate of K two-level chromophores. The electronic ground state of such an aggregate can be described by a product state

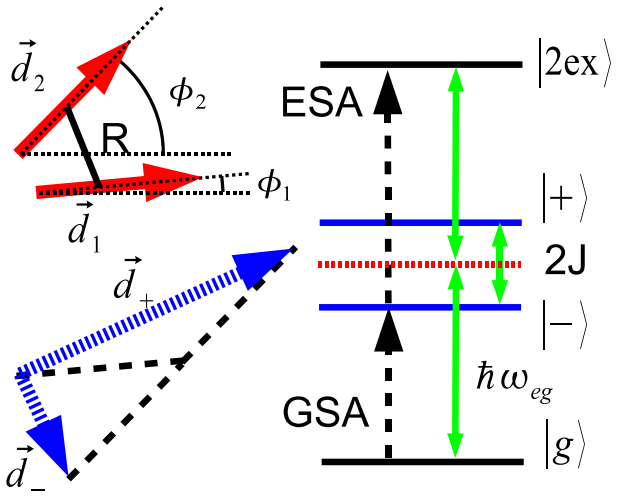

Figure 1: Illustration of the excitonic effect in a homodimer. Electronic excited states $|1\rangle$ and $|2\rangle$ with transition energy $\hbar\omega_{eg}$ localized on the individual molecules (depicted by their transition dipole vectors $\boldsymbol{d}_1$ and $\boldsymbol{d}_2$) form delocalized eigenstates $|+\rangle$ and $|-\rangle$ of the total electronic Hamiltonian. The result of excitonic interaction in a homodimer is splitting of transition energies by twice the resonance interaction J, and consequently an offset of ESA with respect to ground state absorption. The delocalized states have new transition dipole moments $\boldsymbol{d}_+$ and $\boldsymbol{d}_-$ corresponding to a sum and a difference of $\boldsymbol{d}_1$ and $\boldsymbol{d}_2$, respectively.

$$|g\rangle \equiv |g_1 \dots g_K\rangle \equiv |g_1\rangle|g_2\rangle \dots |g_K\rangle, \tag{1}$$

where the state $|g_i\rangle$ is the ground state of the $i-$th monomeric chromophore. Excited states of the aggregate can be constructed using monomeric excited states $|e_i\rangle$. Thus, we will represent single- and double-excitation states as

$$|n\rangle \equiv |g_1 g_2 \dots e_n \dots g_K\rangle, \tag{2}$$

$$|N\rangle \equiv |(n,m)\rangle \equiv |g_1 \dots e_n \dots e_m \dots g_K\rangle, \quad n < m. \tag{3}$$

Excited states with more than two excitation will not be considered as they can often be neglected in the first (linear) and third order spectroscopic experiments that we have in mind here. Unless stated otherwise, we will use capital letters to denote a double-excitation index, e.g. $A = (a,b)$, and lower case letters to denote one-excitation states. The diad (a,b) will be used to denote two-excitation states when the knowledge of the underlying one-excitation states is required. Also sums over double-excitation states will be used $\sum_A$ or $\sum_{(a,b)}$ with the meaning of $\sum_{a=1}^{K}\sum_{b=a+1}^{K}$.

Individual chromophores are described by their ground- and excited state electronic energies ϵ_i^g and ϵ_i^e,

nuclear potential energy surfaces of the ground- and excited states $V_i^g(Q)$ and $V_i^e(Q)$ and the nuclear kinetic energy $T_i(P)$. If we assume for a while that individual chromophores in the aggregate do not interact we arrive at the following Hamiltonian

$$H_0 = H_B + H_{el}, \tag{4}$$

where

$$H_{el} = \epsilon_g |g\rangle\langle g| + \sum_{n=1}^{K} \left(\epsilon_n + \langle V_n(Q) - V_g(Q)\rangle\right) |n\rangle\langle n|$$

$$+ \sum_{N=1}^{K(K-1)/2} \left(\epsilon_N + \langle V_N(Q) - V_g(Q)\rangle\right) |N\rangle\langle N|, \tag{5}$$

and

$$H_B = \left(T(P) + V_g(Q)\right) |g\rangle\langle g|$$

$$+ \sum_{n=1}^{K} \left(V_n(Q) - \langle V_n(Q) - V_g(Q)\rangle\right) |n\rangle\langle n|$$

$$+ \sum_{N=1}^{K(K-1)/2} \left(V_N(Q) - \langle V_N(Q) - V_g(Q)\rangle\right) |N\rangle\langle N|. \tag{6}$$

Here, we introduced

$$T(P) = \sum_{i=1}^{K} T_i(P),\ V_g(Q) = \sum_{i=1}^{K} V_i^g(Q), \tag{7}$$

$$V_n(Q) = \sum_{i\neq n}^{K} V_i^g(Q) + V_n^e(Q),\ V_{N=(k,l)}(Q)$$

$$= \sum_{i\neq k,l}^{K} V_i^g(Q) + V_k^e(Q) + V_l^e(Q). \tag{8}$$

The mean value of the difference between the potential energy in the state denoted by index α and potential energy in the electronic ground state was denoted as

$$\langle V_\alpha(Q) - V_g(Q)\rangle = Tr_Q\{(V_\alpha(Q) - V_g(Q))W_{eq}\}, \tag{9}$$

where $\alpha = n, N$. The density operator W_{eq} represents the equilibrium state of the nuclear DOF in the electronic ground state.

Introducing excitonic interaction, the total Hamiltonian reads

$$H = H_0 + H_J, \tag{10}$$

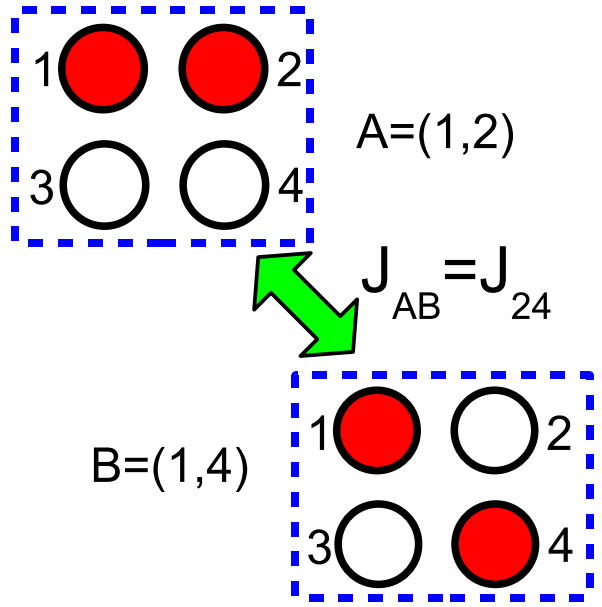

Figure 2: Coupling between two two-excitation states $A = (1,2)$ and $B = (1,4)$. The coupling J_{24} enables transition between the two states, while the one-excitation state 1 is shared.

$$H_J = \sum_{nm} J_{nm} |n\rangle\langle m| + \sum_{NM} J_{NM} |N\rangle\langle M|. \tag{11}$$

For two distinct double-excitation states $M = (m,n)$ and $N = (k,l)$ we assume the following *ansatz* for the resonance coupling

$$J_{MN} = J_{(m,n)(k,l)} = \delta_{mk} J_{nl} + \delta_{nl} J_{mk}$$

$$+ \delta_{ml} J_{nk} + \delta_{nk} J_{ml}. \tag{12}$$

The *ansatz* is schematically described in Fig. 2 which demonstrates how two two-exciton states transfer from one to another by a transition of one excitation, while the other is shared by both double-excitation states.

It is important to note that due to the resonance coupling Hamiltonian, H_J, neither the single- nor double-excitation states are eigenstates of the total electronic Hamiltonian. The actual eigenstates of the electronic Hamiltonian (obtained by its diagonalization) can be expressed as linear combinations of the single- and double-excitation states, and they are usually termed one- and two-exciton states, respectively.

III. EQUATIONS OF MOTION

A. Projection operator method

We start investigation of the dynamics of the molecular aggregates with the Liouville–von Neuman equation for

the total density matrix $W(t)$,

$$\frac{\partial}{\partial t}W(t) = -i\mathcal{L}W(t). \tag{13}$$

Here, we defined the Liouville superoperator (or Liouvillian) $\mathcal{L}A = \frac{1}{\hbar}[H, A]$. The total Liouvillian can be written in terms of the system and the resonance interaction Liouvillians

$$\mathcal{L} = \mathcal{L}_0 + \mathcal{L}_J. \tag{14}$$

The solution of Eq. (13) can be written in terms of the evolution superoperator $\mathcal{U}(t) = \exp\{-\frac{i}{\hbar}\mathcal{L}t\}$ as $W(t) = \mathcal{U}(t)W(0)$. In interaction picture with respect to $\mathcal{L}_0$, we define

$$\mathcal{L}_J(t) = \mathcal{U}_0^\dagger(t)\mathcal{L}_J\mathcal{U}_0(t), \tag{15}$$

and

$$W^{(I)}(t) = \mathcal{U}_0^\dagger(t)W(0), \tag{16}$$

where $\mathcal{U}_0(t) = \exp\{-\frac{i}{\hbar}\mathcal{L}_0 t\}$. Using the usual projection operator method ($P^2 = P$, $Q = 1 - P$) we get

$$\frac{\partial}{\partial t}PW^{(I)}(t) = -iP\mathcal{L}_J(t)PW^{(I)}(t) - iP\mathcal{L}_J(t)QW(t_0)$$

$$-\int_{t_0}^{t} d\tau P\mathcal{L}_J(t)Q\mathcal{L}_J(\tau)PW^{(I)}(\tau), \tag{17}$$

where we have already truncated the perturbation expansion in $\mathcal{L}_J$ at the second order. Although Eq. (17) is valid for an arbitrary projector P, for the quality of the second order approximation, the choice of projection operator P is crucial. The best guidance to this choice is provided by the physical conditions at which the equation is applied. In optical spectroscopy, we often deal with systems that are in the electronic ground state at the initial time, and the bath DOF are relaxed into the canonical equilibrium. Thus, $W(t_0) = |g\rangle\langle g|W_{eq} = \rho_{gg}W_{eq}$. According to the Condon principle, the bath part of this initial condition is not changed upon an ultrafast photo-excitation and the initial condition for relaxation of the nuclear DOF is still given by a canonical density matrix. As a result, the projection operator

$$PA = Tr_Q\{A\}W_{eq}, \tag{18}$$

has the convenient property $QW(t_0) = 0$, and the so-called initial term $iP\mathcal{L}_J(t)QW(t_0)$ is identically equal to zero. This is equivalent to the statement that the projection by P does not lead to a loss of information about the system at t_0.

Another physically important situation occurs when the system has already spent some time in the electronically excited state, and the bath DOF at an excited electronic state $|a\rangle$ has relaxed into local equilibrium represented by the density matrix W_{eq}^a. The projection operator which eliminates the initial term is

$$PA = \sum_a \langle a|Tr_Q\{A\}|a\rangle W_{eq}^a|a\rangle\langle a|. \tag{19}$$

This discussion shows that, in general, it would be desirable that the projection operator P were time-dependent. It is indeed possible to formulate corresponding time-dependent projection operator technique rigorously (see e.g. Ref. [29]). In this contribution, we will not discuss such a time evolution of the projection operator, and we will keep in mind that the present formulation is valid only for not too long relaxation times. We will however discuss Eq. (17) with projection operator, Eq. (19), later in Section IV to demonstrate the relation between the theory developed here and the FRET.

The main feature of the present theory is that the resonance coupling Hamiltonian H_J is the term with respect to which we apply perturbation theory. If the perturbation theory is applied with respect to the system–bath interaction Hamiltonian with projection operator given by Eq. (18), we arrive at the Redfield type relaxation equations (see e.g. [30]), while using the projector, Eq. (19), leads to so-called Modified Redfield equations [31, 32].

B. Projector vs. interaction picture

Eq. (17) is an equation of motion for the RDM. However, the projection operator is applied to the interaction picture density matrix $W^{(I)}(t)$ and not to $W(t)$ as one would expect. We therefore need to express the evolution of $\rho(t) = Tr_Q\{W(t)\}$ in terms of the evolution of $\bar{\rho}(t) = Tr_Q\{W^{(I)}(t)\}$. Because Hamiltonian operators H_{el} and H_B act on different Hilbert spaces, they commute and we can write

$$\bar{\rho}(t) = U_{el}^\dagger(t)Tr_Q\{U_B^\dagger(t)W(t)U_B(t)\}U_{el}(t). \tag{20}$$

Matrix elements $\bar{\rho}_{ab}(t)$ of the RDM therefore read

$$\bar{\rho}_{ab}(t) = e^{i\omega_{ab}t}Tr_Q\{U_a^\dagger(t)W_{ab}(t)U_b(t)\}. \tag{21}$$

Due to the properties of the trace operation, we find that for populations

$$\bar{\rho}_{aa}(t) = \rho_{aa}(t). \tag{22}$$

For the coherences $\bar{\rho}_{ab}(t)$, $a \neq b$ it is not possible to write directly such a simple result. However, an approximate relation between the two RDMs can be established by studying the case where $H_J = 0$. In this case, $W_{ab}(t) = U_B(t)W_{eq}U_B^\dagger(t)$ and $\bar{\rho}_{ab}(t) = \bar{\rho}_{ab}(0)$, because all the time evolution was accounted for by the interaction picture. At the same time, however, we can show that in second cumulant approximation

$$\rho_{ab}(t) = \rho_{ab}(0)e^{-i\omega_{ab}t - g_a(t) - g_b^*(t)},\ a \neq b, \tag{23}$$

where $g_a(t)$ is the well-known line shape function associated with the transition $|g_a\rangle \to |e_a\rangle$[20]. Thus, because the purpose of the interaction picture is to suppress the time evolution due to Hamiltonian H_0 we can write

$$\bar{\rho}_{ab}(t) = e^{i\omega_{ab}t + (1-\delta_{ab})[g_a(t) + g_b^*(t)]}\rho_{ab}(t), \tag{24}$$

so that the exponential prefactor compensates the "J-free" evolution of the RDM elements in the spirit of the interaction picture.

C. Reduced density matrix equations

We can now rewrite Eq. (17) in second order in terms of $\bar{\rho}(t)$ as

$$\frac{\partial}{\partial t}\bar{\rho}(t)W_{eq} = -iTr_Q\{H_J(t)W_{eq}\}\bar{\rho}(t)W_{eq}$$

$$+ i\bar{\rho}(t)Tr_Q\{W_{eq}H_J(t)\}W_{eq} + R(J^2), \qquad (25)$$

where

$$R(J^2) = \int_{t_0}^{t} d\tau P\mathcal{L}_J(t)Q\mathcal{L}_J(\tau)PW^{(I)}(\tau). \qquad (26)$$

In this subsection, let us use the lower case indices to denote both the one- and two-excitation states. The traces in Eq. (25) can be easily evaluated in second order cumulant approximation

$$\langle a|Tr_Q\{H_J(t)W_{eq}\}|b\rangle = J_{ab}e^{i\omega_{ab}t}Tr_Q\{U_a^\dagger(t)U_b(t)W_{eq}\}$$

$$= J_{ab}e^{i\omega_{ab}t-(1-\delta_{ab})[g_a^*(t)+g_b(t)]} \equiv J_{ab}(t), \qquad (27)$$

and we arrive at

$$\frac{\partial}{\partial t}\bar{\rho}_{ab}(t) = -\frac{i}{\hbar}\sum_c J_{ac}(t)\bar{\rho}_{cb}(t)$$

$$+ \frac{i}{\hbar}\sum_c \bar{\rho}_{ac}(t)J_{cb}(t) - R(J^2)/W_{eq}. \qquad (28)$$

In the second order term, Eq. (26), we have to evaluate two commutators of Hamiltonian H_J with the reduced density matrix

$$R(J^2)/W_{eq} = \frac{1}{\hbar^2}\int_{t_0}^{t} d\tau\Big[Tr_Q\{H_J(t)H_J(\tau)W_{eq}\}\bar{\rho}(\tau)$$

$$-Tr_Q\{H_J(t)W_{eq}\}Tr_Q\{H_J(\tau)W_{eq}\}\bar{\rho}(\tau)$$

$$-Tr_Q\{H_J(t)\bar{\rho}(\tau)W_{eq}H_J(\tau)\}$$

$$+Tr_Q\{H_J(t)W_{eq}\}\bar{\rho}(\tau)Tr_Q\{W_{eq}H_J(\tau)\}$$

$$-Tr_Q\{H_J(\tau)\bar{\rho}(\tau)W_{eq}H_J(t)\}$$

$$+Tr_Q\{H_J(\tau)W_{eq}\}\bar{\rho}(\tau)Tr_Q\{W_{eq}H_J(t)\}$$

$$+\bar{\rho}(\tau)Tr_Q\{W_{eq}H_J(\tau)H_J(t)\}$$

$$-\bar{\rho}(\tau)Tr_Q\{W_{eq}H_J(\tau)\}Tr_Q\{W_{eq}H_J(t)\}\Big]. \qquad (29)$$

The matrix elements involved in Eq. (29) read in detail

$$\langle a|Tr_Q\{H_J(t)H_J(\tau)W_{eq}\}|b\rangle = \sum_c J_{ac}J_{cb}e^{i\omega_{ac}t+i\omega_{cb}\tau}$$

$$\times Tr_Q\{U_a^\dagger(t)U_c(t)U_c^\dagger(\tau)U_b(\tau)W_{eq}\}, \qquad (30)$$

$$\langle a|Tr_Q\{H_J(t)|c\rangle\ldots W_{eq}\langle d|H_J(\tau)\}|b\rangle = J_{ac}\ldots J_{db}$$

$$\times e^{i\omega_{ac}t+i\omega_{dc}\tau}Tr_Q\{U_a^\dagger(t)U_c(t)W_{eq}U_d^\dagger(\tau)U_b(\tau)\} \qquad (31)$$

and

$$\langle a|Tr_Q\{W_{eq}H_J(\tau)H_J(t)\}|b\rangle = \sum_c J_{ac}J_{cb}e^{i\omega_{ac}\tau+i\omega_{cb}t}$$

$$\times Tr_Q\{U_a^\dagger(\tau)U_c(\tau)U_c^\dagger(t)U_b(t)W_{eq}\}. \qquad (32)$$

We introduce an auxiliary function

$$M_{abcd}(t,\tau) = Tr_Q\{U_a^\dagger(t)U_b(t)$$

$$\times U_c^\dagger(\tau)U_d(\tau)W_{eq}\}e^{i\omega_{ab}t+i\omega_{cd}\tau}, \qquad (33)$$

with the property

$$M_{abcd}(t,\tau) = M_{dcba}^*(\tau,t) \qquad (34)$$

and after changing the integration variable to $\tau' = t-\tau$ we can write the EM in the form

$$\frac{\partial}{\partial t}\bar{\rho}_{ab}(t) = -\frac{i}{\hbar}\sum_c J_{ac}(t)\bar{\rho}_{cb}(t)$$

$$+\frac{i}{\hbar}\sum_c \bar{\rho}_{ac}(t)J_{cb}(t) - \sum_{cd}\frac{1}{\hbar^2}\int_0^{t-t_0} d\tau$$

$$[J_{ac}J_{cd}M_{accd}(t,t-\tau) - J_{ac}(t)J_{cd}(t-\tau)]\,\bar{\rho}_{db}(t-\tau)$$

$$-[J_{ca}^*J_{bd}^*M_{cabd}^*(t,t-\tau) - J_{ca}^*(t)J_{bd}^*(t-\tau)]\,\bar{\rho}_{cd}(t-\tau)$$

$$-[J_{db}J_{ac}M_{dbac}(t,t-\tau) - J_{db}(t)J_{ac}(t-\tau)]\,\bar{\rho}_{cd}(t-\tau)$$

$$+[J_{bd}^*J_{dc}^*M_{bddc}^*(t,t-\tau)$$

$$- J^*_{bd}(t)J^*_{dc}(t-\tau)]\bar{\rho}_{ac}(t-\tau). \quad (35)$$

This is a form suitable for introducing both long time limit ($t_0 \to \infty$) and the Markov approximation ($\bar{\rho}_{ab}(t-\tau) \approx \bar{\rho}_{ab}(t)$). We apply only the later one, because we are interested mostly in short times. Now, it only remains to evaluate the four-index matrix $M_{abcd}(t,\tau)$ which is done in Appendix A using the cumulant expansion. In Markov approximation, we can write our equations as

$$\frac{\partial}{\partial t}\bar{\rho}_{ab}(t) = -\frac{i}{\hbar}\sum_c J_{ac}(t)\bar{\rho}_{cb}(t)$$

$$+\frac{i}{\hbar}\sum_c \bar{\rho}_{ac}(t)J_{cb}(t) - \sum_{cd}\Big[R_{accd}(t)\bar{\rho}_{db}(t) - R^*_{cabd}(t)\bar{\rho}_{cd}(t)$$

$$- R_{dbac}(t)\bar{\rho}_{cd}(t) + R^*_{bddc}(t)\bar{\rho}_{ac}(t)\Big], \quad (36)$$

where we introduced relaxation tensor

$$R_{abcd}(t) = \frac{1}{\hbar^2}\int_0^t d\tau\Big[J_{ab}J_{cd}M_{abcd}(t,t-\tau)$$

$$- J_{ab}(t)J_{cd}(t-\tau)\Big]. \quad (37)$$

We derived EM of the RDM in the interaction picture. We use Eq. (24) to transform the RDM in Schrödinger picture if necessary. The first two terms in Eq. (36) correspond to the delocalization effect of resonance coupling given by Eq. (27). While the term $e^{i\omega_{ab}t}$ in Eq. (27) originates from the interaction picture with respect to the electronic Hamiltonian, the presence of the line-shape functions in Eq. (27) shows that the magnitude of this coupling decreases exponentially with growing time t. Thus the bath fluctuations dynamically destroys the resonance coupling.

D. Two-excitation states

In higher order spectroscopies, ESA contributes considerably to the signal. A delicate balance of ground state bleaching and stimulated emission on one hand, and the ESA on the other hand, is behind the disappearance of the 2D crosspeaks when resonance coupling goes to zero. For weakly coupled aggregates, correct description of ESA, and correspondingly the dephasing of coherences between one-excitation and two-excitation state is indispensable.

In this subsection, let us again denote one-excitation and two-excitation states by the lower case and the upper case letters, respectively. The evolution of the system in a two-exciton state $A = (a,b)$ is described by the evolution operator

$$U_A(t) = \exp\left\{-\frac{i}{\hbar}H_A t\right\}$$

$$= \exp\left\{-\frac{i}{\hbar}[H_a \otimes 1_{\{a\}} + 1_{\{b\}} \otimes H_b]t\right\}, \quad (38)$$

i.e.

$$U_A(t) = U_a(t) \otimes U_b(t) \otimes 1_{\{a,b\}}. \quad (39)$$

We denoted the direct product of unity operators from Hilbert spaces except of those in a set $\{a,b,\ldots\}$ by $1_{\{a,b,\ldots\}}$. Expressions containing a product $U_A(t)U^\dagger_B(t)$, where one of the excited states is shared by the two-exciton states A and $B = (a,c)$, thus yield

$$U_{(a,b)}(t)U^\dagger_{(a,c)}(t) = 1_{\{b,c\}} \otimes U_b(t)U^\dagger_c(t). \quad (40)$$

Considering the first order term and a general case $M = (m,n)$, $N = (k,l)$ one arrives at

$$J_{MN}(t) = J_{MN}e^{i\omega_{MN}t}Tr_Q\{U^\dagger_M(t)U_N(t)W_{eq}\}$$

$$= \delta_{mk}J_{nl}(t) + \delta_{nl}J_{mk}(t) + \delta_{ml}J_{nk}(t) + \delta_{nk}J_{ml}(t). \quad (41)$$

For the terms in the second order of J we have in a complete analogy

$$J_{MN}J_{cd}M_{MNcd}(t,\tau) =$$

$$\delta_{mk}J_{nl}J_{cd}M_{nlcd}(t,\tau) + \delta_{nl}J_{mk}J_{cd}M_{mkcd}(t,\tau)$$

$$+ \delta_{ml}J_{nk}J_{cd}M_{nkcd}(t,\tau) + \delta_{nk}J_{ml}J_{cd}M_{mlcd}(t,\tau), \quad (42)$$

and consequently

$$R_{MNcd}(t) = \delta_{mk}R_{nlcd}(t) + \delta_{nl}R_{mkcd}(t)$$

$$+ \delta_{ml}R_{nkcd}(t) + \delta_{nk}R_{mlcd}(t). \quad (43)$$

Thus, all quantities corresponding to the two-excitation states can be expressed directly using the one-excitation quantities.

E. Homogeneous limit

To evaluate the relaxation tensor we need to evaluate the following two expressions

$$R'_{abcd}(t) = \frac{1}{\hbar^2}J_{ab}J_{cd}\int_0^t d\tau M_{abcd}(t,t-\tau), \quad (44)$$

and

$$R''_{abcd}(t) = -\frac{1}{\hbar^2}J_{ab}(t)\int_0^t d\tau J_{cd}(t-\tau). \quad (45)$$

In order to simplify the equations, we will assume so-called homogeneous limit, where we have

$$g_a(t) = \Gamma_a t. \tag{46}$$

This simple formula allows us to evaluate all terms in the relaxation matrix analytically. First we observe that

$$J_{ab}(t) = J_{ab} e^{-(\Gamma_a+\Gamma_b)t + i\omega_{ab}t}, \tag{47}$$

and therefore

$$R''_{abcd}(t) = J_{ab}J_{cd} e^{-(\Gamma_a+\Gamma_b)t+i\omega_{ab}t} \frac{1}{(\Gamma_c+\Gamma_d) - i\omega_{cd}}$$

$$\times \left(e^{-(\Gamma_c+\Gamma_d)t + i\omega_{cd}t} - 1 \right). \tag{48}$$

The R' elements are obtained in a similar manner. We start with a splitting of the M functions

$$M_{abcd}(t,\tau) = M'_{abcd}(t) M''_{abcd}(t-\tau)$$

$$\times M'''_{abcd}(\tau) e^{i\omega_{ab}t + i\omega_{cd}\tau}. \tag{49}$$

Such a splitting is possible for an arbitrary $g(t)$ function and is not limited to the homogeneous limit. In general, the integrals, Eqs. (44) and (45), can be evaluated using the Fourier transform. In homogeneous limit we find that

$$M'_{abcd}(t) = e^{-\alpha_{abcd}t},\ M''_{abcd}(t) = e^{-\beta_{abcd}t},$$

$$M'''_{abcd}(t) = e^{-\gamma_{abcd}t}, \tag{50}$$

where

$$\alpha_{abcd} = (1 - \delta_{ac} + \delta_{ad})\Gamma_a + (1 - \delta_{bc} - \delta_{bd})\Gamma_b, \tag{51}$$

$$\beta_{abcd} = (\delta_{ad} - \delta_{ac})\Gamma_a + (\delta_{bc} - \delta_{bd})\Gamma_b, \tag{52}$$

and

$$\gamma_{abcd} = \Gamma_c + \Gamma_d + (\delta_{ac} - \delta_{ad})\Gamma_a + (\delta_{bd} - \delta_{bc})\Gamma_b. \tag{53}$$

Using the definition, Eq. (44), we get

$$R'_{abcd}(t) = J_{ab}J_{cd} e^{i(\omega_{ab}+\omega_{cd})t - (\alpha_{abcd}+\gamma_{abcd})t}$$

$$\times \frac{1}{\gamma_{abcd} - \beta_{abcd} - i\omega_{cd}} \left[e^{(\gamma_{abcd}-\beta_{abcd})t - i\omega_{cd}t} - 1 \right]. \tag{54}$$

The case when $\gamma_{abcd} - \beta_{abcd} - i\omega_{cd} = 0$, which can occur for homo aggregates, has to be considered separately. According to Eqs. (44) and (49), when the denominator is equal to zero, the dependence on the integration variable disappears and the integral leads to t. Consequently,

$$R'_{abcd}(t) = J_{ab}J_{cd} t e^{i(\omega_{ab}+\omega_{cd})t - (\alpha_{abcd}+\gamma_{abcd})t}. \tag{55}$$

If the dephasing constants Γ are non-zero, no such problem can occur with Eq. (48).

We stress that the homogeneous limit is used here for demonstration purposes only. The line broadening function, Eq. (46), corresponds to a limit of ultrafast stochastic bath with correlation function $C(t) = \Gamma\delta(t)$. Such correlation function does not allow for introducing required thermodynamic properties $C(\omega) = e^{\hbar\omega/k_BT} C(-\omega)$ for the corresponding spectral density $C(\omega) = \int_{-\infty}^{\infty} dt C(t) e^{i\omega t}$. Consequently, the relaxation tensor given by Eqs. (48) and (54) does not lead to any finite temperature thermal equilibrium. We will treat calculations with realistic correlation functions elsewhere.

IV. LONG-TIME LIMIT OF EQUATIONS OF MOTION

In order to establish the relation between our EM, Eq. (36), and standard EM used to describe dissipative dynamics and energy transfer, we show that the above derivation leads to the well-know Förster resonance transfer rates in the long time limit. Considering the projection operator, Eq. (19), we first find that

$$P\mathcal{L}_J(t) P W^{(I)}(t) = 0, \tag{56}$$

which leads also to

$$P\mathcal{L}_J(t) Q \mathcal{L}_J(\tau) P W^{(I)}(\tau)$$

$$= P\mathcal{L}_J(t) \mathcal{L}_J(\tau) P W^{(I)}(\tau). \tag{57}$$

Using the definition of the projection operator, Eq. (19), Eq. (17) turns into

$$\frac{\partial}{\partial t}\rho_{aa}(t) = -\frac{1}{\hbar^2} \sum_b |J_{ab}|^2$$

$$\times \int_{t_0}^{t} d\tau \Big[\{C^*_{ba}(t-\tau) + C_{ba}(t-\tau)\} \rho_{aa}(\tau)$$

$$- \{C_{ab}(t-\tau) + C^*_{ab}(t-\tau)\} \rho_{bb}(\tau) \Big], \tag{58}$$

where

$$C_{ab}(t) = Tr_Q \left\{ U_a(t) U_b^\dagger(t) W_{eq}^{ab} \right\}. \tag{59}$$

The initial state of the bath W_{eq}^{ab} is the one in which chromophore b is vibrationally relaxed in the electronically excited state, and a is relaxed the electronic ground-state. Thus, $W_{eq}^{ab} = W_{eq}^g W_{eq}^b$. We apply the second order cumulant expansion and get

$$C_{ab}(t) = Tr_Q \left\{ U_a(t) U_g^\dagger(t) W_{eq}^q \right\} Tr_Q \left\{ U_g(t) U_b^\dagger(t) W_{eq}^b \right\}$$

$$= e^{-g_a(t)-i\omega_{ag}t}e^{-g_b^*(t)+i(\omega_{bg}-2\lambda_b)t}, \quad (60)$$

where we used the property $2\lambda_a = Tr_Q\{\Delta V_a W_g^{eq}\} - Tr_Q\{\Delta V_a W_a^{eq}\}$ (see e.g. Ref. [20]). By substitution $\tau' = t - \tau$, limit $t_0 \to -\infty$ and Markov approximation $\rho_{aa}(t-\tau') \approx \rho_{aa}(t)$ we obtain relaxation rate equation with Förster rates (see e.g. Ref. [32])

$$K_{a\leftarrow b} = 2Re\left|\frac{J_{ab}}{\hbar}\right|^2$$

$$\times \int_0^\infty d\tau e^{-g_a(\tau)-i\omega_{ag}t-g_b^*(\tau)+i(\omega_{bg}-2\lambda_b)\tau}. \quad (61)$$

This demonstrates the relation of Eq. (36) to the Förster energy transfer rates. It is important to point out that the only difference between the two sets of equations is in the "initial" condition set on the bath part of the density matrix by the choice of the projection superoperator. Thanks to our choice of the projection operator, equations used in this work retain the description of the electronic coherences, while Förster rate equations give no prescription for them.

V. ABSORPTION AND TWO-DIMENSIONAL CORRELATION PHOTON ECHO SPECTRA

To calculate optical spectra we concentrate on coherence elements of the RDM that correspond to optical transitions. We apply perturbation theory with respect to electric field of an incident light to calculate absorption and two-dimensional correlation photon echo spectra [20].

A. Optical coherences

To calculate response functions needed for evaluations of optical spectra in general, we need first to calculate evolution operators $\mathcal{U}(t)$ which fulfill the relation

$$\rho(t) = \mathcal{U}(t)\rho(0). \quad (62)$$

We use a simple consequence of this equation, namely

$$\mathcal{U}_{abcd}(t) = \rho_{ab}(t), \quad (63)$$

where $\rho_{ab}(t)$ is calculated using EM, Eq. (36), with initial condition $\rho_{ab}(0) = \delta_{ac}\delta_{bd}$.

If any of the indices a, b, c, d equals g, we have $R_{abcd} = 0$. For the optical coherences involving the ground state we therefore obtain the following EM

$$\frac{\partial}{\partial t}\bar{\rho}_{ag}(t) = -\sum_c \frac{i}{\hbar}J_{ac}(t)$$

$$+\sum_c\sum_{d\neq a,c} R_{addc}(t)\bar{\rho}_{cg}(t). \quad (64)$$

Also, when both the single and double excited states are present in the R_{abcd} matrix, many elements of the matrix are zero, most importantly those where e.g. a and b are a single excitation and double excitation indices, respectively. For the coherences involving the one exciton and two exciton states we have EM

$$\frac{\partial}{\partial t}\bar{\rho}_{aB}(t) = -\frac{i}{\hbar}\sum_c J_{ac}(t)\bar{\rho}_{cB}(t) + \frac{i}{\hbar}\sum_C \bar{\rho}_{aC}(t)J_{CB}(t)$$

$$-\sum_{cd} R_{accd}(t)\bar{\rho}_{dB}(t) + \sum_{cD}\left[R^*_{caBD}(t) + R_{DBac}(t)\right]\bar{\rho}_{cD}(t)$$

$$-\sum_{CD} R^*_{BDDC}(t)\bar{\rho}_{aC}(t). \quad (65)$$

It is possible to rewrite this equation entirely using the one-excitation indices by considering Eqs. (41) and (43). Setting $B = (\sigma, \pi)$, $D = (\gamma, \delta)$ and $C = (\alpha, \beta)$ yields

$$\frac{\partial}{\partial t}\bar{\rho}_{a(\sigma\pi)}(t) = -\frac{i}{\hbar}\sum_c J_{ac}(t)\bar{\rho}_{c(\sigma\pi)}(t)$$

$$-\sum_{cd} R_{accd}(t)\bar{\rho}_{d(\sigma\pi)}(t) + \mathcal{T}_1 + \mathcal{T}_2 - \mathcal{T}_3, \quad (66)$$

where last three terms $\mathcal{T}_1$, $\mathcal{T}_2$ and $\mathcal{T}_3$ are somewhat lengthy. We present the first term here,

$$\mathcal{T}_1 = \frac{i}{\hbar}\Big[\sum_{\beta=\sigma+1}^{K}\bar{\rho}_{a(\sigma\beta)}(t)J_{\beta\pi}(t) + \sum_{\alpha=1}^{\pi-1}\bar{\rho}_{a(\alpha\pi)}(t)J_{\alpha\sigma}(t)$$

$$+\sum_{\beta=\pi+1}^{K}\bar{\rho}_{a(\pi\beta)}(t)J_{\beta\sigma}(t) + \sum_{\alpha=1}^{\sigma-1}\bar{\rho}_{a(\alpha\sigma)}(t)J_{\alpha\pi}(t)\Big], \quad (67)$$

and the remaining two are presented in full in the Appendix. From the point of view of simulation feasibility, Eq. (66) represents the main advantage of treating a weakly coupled excitonic systems in the site basis, as opposed to the treatment in the excitonic basis. Although Eq. (66) is rather lengthy, one is concerned only with tensor quantities with the number of elements proportional to $\sim N^4$, where N is the number of chromophores, as opposed to $\sim N^6$ which would be required in excitonic basis.

B. Absorption spectrum

The absorption spectrum is given by expression

$$\alpha(\omega) \approx \frac{\omega}{n(\omega)}Re\int_0^\infty dt e^{i\omega t}$$

$$\times \left\langle \sum_{ab} d_{ga}\mathcal{U}_{agbg}(t)d_{bg}\rho_{gg} \right\rangle, \quad (68)$$

where $\langle \ldots \rangle$ represents an averaging over isotropic distribution of orientations of the molecular transitions with respect to the light polarization. The transition dipole moments d_{ag} have to be understood as projections of the transition dipole moments on the light polarization vector $\mathbf{e}$, i.e. $d_{ag} = \mathbf{d}_{ag} \cdot \mathbf{e}$. The averaging is done over a product of two of such quantities. We have

$$\Omega_{ab} \equiv \langle (\mathbf{d}_{ag} \cdot \mathbf{e})(\mathbf{d}_{bg} \cdot \mathbf{e}) \rangle_{orient.} = \frac{1}{3} \frac{\mathbf{d}_{ag} \cdot \mathbf{d}_{bg}}{|\mathbf{d}_{ag}||\mathbf{d}_{bg}|}. \quad (69)$$

If one now defines $\bar{d}_{ag}$ to $\bar{d}_{ag} \equiv |\mathbf{d}_{ag}|$ one can write

$$\alpha(\omega) \approx \frac{\omega}{n(\omega)} Re \int_0^\infty dt e^{i\omega t}$$

$$\times \sum_{ab} \Omega_{ab}\bar{d}_{ga}\bar{d}_{bg}\mathcal{U}_{agbg}(t)\rho_{gg}. \quad (70)$$

We use Eq. 70 in subsequent simulations of absorption spectra. It is important to note that because we do not work with electronic eigenstates one cannot assume the so-called secular approximation ($\mathcal{U}_{abcd}(t) = \delta_{ac}\delta_{bd}\mathcal{U}_{abab}(t)$) to be valid, and the orientational factor does not reduce to simple 1/3.

C. Two-dimensional spectrum

Two-dimensional (2D) Fourier transformed photon echo (FTPE) spectroscopy is well described by the third order time dependent perturbation theory with respect to light-matter interaction [20]. The spectroscopic signals are expressed in terms of response functions corresponding to light-matter interaction events. These response function allow us to calculate an arbitrary third order response of a multi-level electronic system, provided we know the evolution superoperators $\mathcal{U}$ and the transition dipole moment elements d_{ij}, for all involved electronic levels. The response functions are directly proportional to the observed signal if the incident pulses are infinitely short. Expressions for all response functions R_{ig} and R_{if} ($i = 1, \ldots 4$) involved in the calculations of the 2D FTPE of our model systems are summarized in Appendix VII.

In this paper we will consider only 2D spectra with zero population time, $t_2 = 0$. The impulsive limit signals in the rephasing and non-rephasing configuration can be obtained as follows (see e.g. [33])

$$S_R(t_3, t_1) = R_{2g}(t_3, 0, t_1)$$

$$+ R_{3g}(t_3, 0, t_1) - R^*_{1f}(t_3, 0, t_1), \quad (71)$$

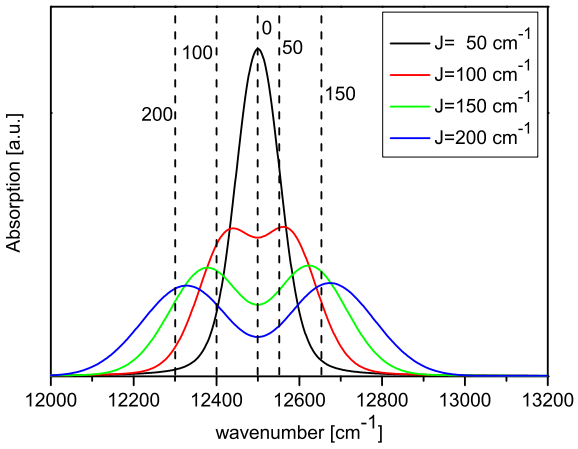

Figure 3: Illustration of excitonic splitting in a model homodimer system. Linear absorption spectrum of a homodimer with perpendicular transition dipole moments calculated using Eq. (70). The following parameters were used to illustrate the influence of resonance coupling: $\epsilon_1 = \epsilon_2 = 12500$ cm^{-1}, resonance coupling $J = 50$, 100, 150 and 200 cm^{-1}, and $\Gamma = 1/400$ fs^{-1}.

and

$$S_{NR}(t_3, t_1) = R_{1g}(t_3, 0, t_1)$$

$$+ R_{4g}(t_3, 0, t_1) - R_{2f}(t_3, 0, t_1). \quad (72)$$

The total signal is given by

$$S(t_3, t_1) = \Theta(t_1)S_R(t_3, t_1) + \Theta(-t_1)S_{NR}(t_3, -t_1), \quad (73)$$

and consequently, the 2D spectrum, which is defined as a double Fourier transform of the signal $S(t_3, t_1)$ is given by [33]

$$\Xi(\omega_3, \omega_1) = \int_0^\infty dt_3 \int_0^\infty dt_1 S_R(t_3, t_1)e^{i\omega_3 t_3 - i\omega_1 t_1}$$

$$+ \int_0^\infty dt_3 \int_0^\infty dt_1 S_{NR}(t_3, t_1)e^{i\omega_3 t_3 + i\omega_1 t_1}. \quad (74)$$

In each response function component of the 2D spectrum, Fourier transform can be performed in t_1 and t_3 times separately.

VI. RESULTS AND DISCUSSION

The theory developed in the above sections has been implemented in the spectroscopic package NOSE [34]

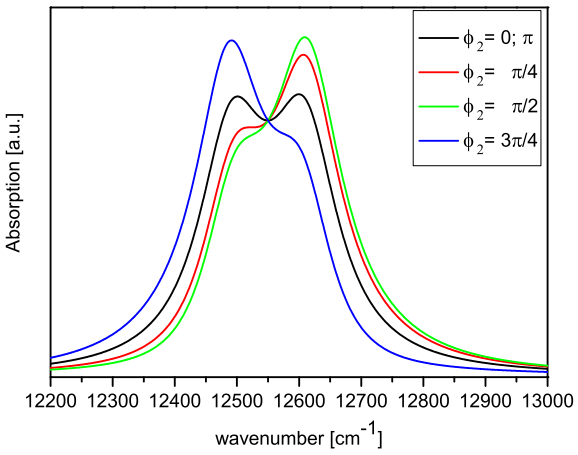

Figure 4: Illustration of oscillator strength redistribution due to resonance coupling in a model heterodimer. The mutual position and orientation of the transition dipoles are described by angles ϕ_1 and ϕ_2 from Fig. 1. The parameters of the model are $\epsilon_1 = 12500$ cm^{-1}, $\epsilon_2 = 12600$ cm^{-1}, $J = 50$ cm^{-1}, $\Gamma = 1/100$ fs^{-1}, $\phi_1 = \pi/2$ and $\phi_2 = 0$, $\pi/4$, $\pi/2$, $3\pi/2$ and π.

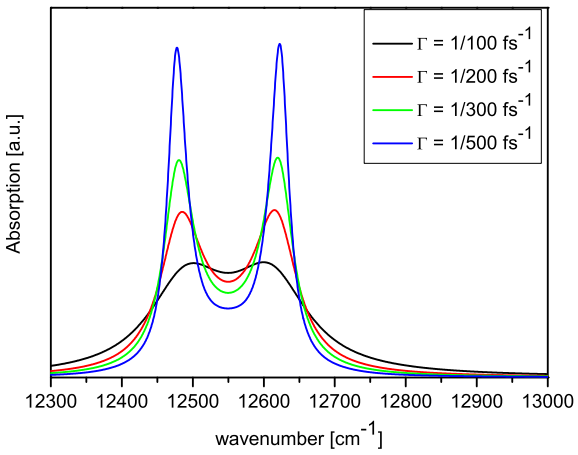

Figure 5: Influence of dephasing on excitonic splitting in a model heterodimer. The parameters of the model are $\epsilon_1 = 12600$ cm^{-1}, $\epsilon_2 = 12500$ cm^{-1}, $J = 50$ cm^{-1}, $\phi_1 = \pi/2$ and $\phi_2 = \pi$. The dephasing rates are $\Gamma = 1/100$, $1/200$, $1/300$ and $1/500$ fs^{-1}.

which was used to perform simulations of impulsive limit 2D spectra of several small model systems. We have chosen systems where effects of weak excitonic coupling, such as those reported in Ref. [14] for LH3 could be expected. We demonstrate below that our local basis description is sufficient to account for such effects. To take advantage of analytic equations derived in earlier sections, we stay in homogeneous limit. Simulations taking advantage of the full description, including a finite bath correlation time will be presented elsewhere.

A. Molecular dimer

The simplest system where a weak excitonic coupling effect in excited state absorption can be observed is a molecular dimer. Resonance interaction leads to the splitting of the excited states, redistribution of the transition dipole moments and a shift of excited state absorption. These effects will be demonstrated here. In addition, one can also expect energy transfer between the two split excitonic levels, formation of a coherence between excitonic levels upon excitation by light and its dephasing. This class of effects is associated with the evolution of the system in the excited state band, and will be studied within our model elsewhere. Fig. 1 illustrates the dimer geometry and its excitonic splitting. In all dimers considered here, transition dipole moments lie in a $z = 0$ plane. Orientation of the dipoles with respect to x and y axes is determined by an angle ϕ such that $d_x = |d| \cos\phi$.

Absorption spectrum of the dimer displays the splitting of the levels, as well as the transition dipole moment redistribution. Fig. 3 presents absorption spectra of a model homo-dimer with resonance coupling varying from 50 cm^{-1} to 200 cm^{-1} and dephasing parameters $\Gamma = 1/400$ fs^{-1}. Because the monomeric transition energies of the two levels are the same, excitonic mixing of the two levels is maximal at any resonance coupling value. We have artificially chosen the dipole moments perpendicular to each other to eliminate the effect of transition dipole moment redistribution. We can see from Fig. 3 that the prediction of the absorption maxima agrees rather well with the prediction of excitonic model (splitting of $2J$). It can also be noticed that the splitting is smaller than predicted by excitonic theory when resonance coupling is small, most likely due to the bath suppressing the exciton coupling term in Eq. (27).

The effect of the transition dipole moment redistribution is illustrated on Fig. 4. A hetero-dimer with difference of 100 cm^{-1} between the transition energies on the two monomers was chosen, and the absorption spectrum was calculated for a fixed resonance coupling value of 50 cm^{-1}. Different mutual orientations of the dipole moments lead to enhancement of the absorption on one or the other split level, depending on mutual orientation of the molecules.

In Fig. 5 we demonstrate that increasing the dephasing rate Γ leads to broadening of the absorption spectrum. Unlike in case of exciton splitting were the position of the line does not shift, here we can observe a small shift towards less pronounced splitting with increasing the dephasing rate.

The effect of excited state absorption offset cannot be demonstrated on an ordinary absorption spectrum. We

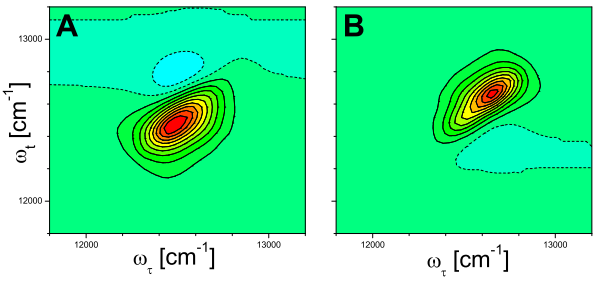

Figure 6: 2D spectrum of a homo dimer. Subfigures: (A) in line configuration with excitonic coupling $J = -80$ cm^{-1}, disorder width $\Delta = 100$ cm^{-1}; (B) sandwich configuration with excitonic coupling $J = 40$ cm^{-1} and $\Delta = 100$ cm^{-1}. Full line contours represent positive values from 10% to 100% of the maximum. Zero and negative contours are dashed, and spaced by 10% of the positive maximum.

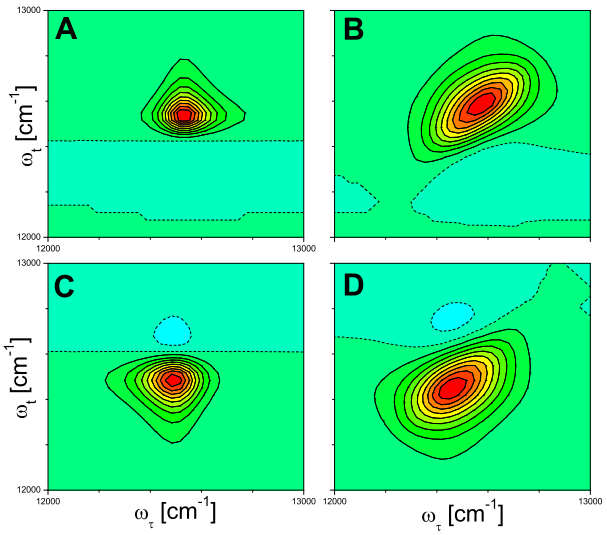

Figure 7: Two-dimensional correlation photon echo spectrum of a model trimer. Subfigures: (A) radial configuration $\alpha = -\frac{\pi}{2}$, single realization; (B) radial configuration, averaged over disorder with $\Delta = 100$ cm^{-1}; (C) tangential configuration $\alpha = 0$, single realization; (D) tangential configuration, averaged over disorder with $\Delta = 100$ cm^{-1}. All site energies are $\epsilon = 12500$ cm^{-1} and $\Gamma = 1/300$ fs^{-1}. Contours as in Fig. 6.

have therefore calculated 2D electronic spectra at population time $t_2 = 0$ for two dimer configurations. An *in line* configuration, Fig. 6A, corresponds to two transition dipole moments oriented head-to-tail with the distance and dipole moment length chosen such that the dipole-dipole coupling leads to $J = -80$ cm^{-1}. This results in an offset of the ESA towards higher frequencies. The *sandwich* configuration with two parallel dipole moments and the same center to center distance results in positive coupling $J = 40$ cm^{-1} . The ESA appears on the lower frequencies (Fig. 6B) in this case. Both calculations are performed with a diagonal Gaussian disorder with the FWHM of $\Delta = 100$ cm^{-1}.

B. Small aggregates

We have also investigated trimers, tetramers and pentamers. As our work is motivated by highly symmetric homo aggregates like LH2 we calculated 2D spectra of aggregates of N monomers with circular $N-$ fold symmetry. Dipole moments are all in plane with the ring formed by the monomers, and we assume an angle α between the tangent touching the circle at the position of the monomer and its transition dipole moment. We compare two cases: $\alpha = 0$ (tangential orientation of the chromophores) and $\alpha = -\frac{\pi}{2}$ (radial orientation with dipoles pointing towards to center of the ring). It was shown in Ref. [35] that these two configurations have a distinct position of the excited state absorption. Fig. 7A presents 2D spectra of an average trimer with $\alpha = 0$, Fig. 7B presents the same trimer calculated averaging over 100 realizations with energetic disorder of $\Delta = 100$ cm^{-1}. The former figure reveals real part of the simple complex Lorentzian lineshape which is a consequence of the homogeneous limit assumed here. The excited state absorption is found below the ground state contribution in this case. For the radial configuration, i.e. $\alpha = -\frac{\pi}{2}$ show on Figs. 7C and 7D the excited state absorption is found above the ground state contribution. If a trimer is considered a member of the family of $N-$fold symmetric aggregates this result is the opposite of the expected effect identified in Ref. [35]. However, trimer has to be considered a special case with respective angles between the chromophores very different from the larger aggregates of the same symmetry. In larger aggregate we can expect that the ESA will be in a position similar to the in line dimer for tangential orientation, and in a position similar to the sandwich dimer for radial orientation. Indeed, already the pentamer follows the rule found for larger circular aggregates. As we can see on Fig. 8 the two configurations have now position of the ESA in agreement with Ref. [35].

Figs. 6 to 8 demonstrate that the theory developed in this paper reproduces correctly the ESA features of 2D spectra of symmetric weakly coupled excitonic aggregates. From the theoretical point of view ESA features are a result of a delicate balance between ESA and GSA contributions which cancel exactly in case of uncoupled chromophores. This feature makes 2D of uncoupled chromophores additive.

C. Additivity of the 2D spectra

We will demonstrate that our theory fulfills the additivity property, and show that the GSA and ESA contri-

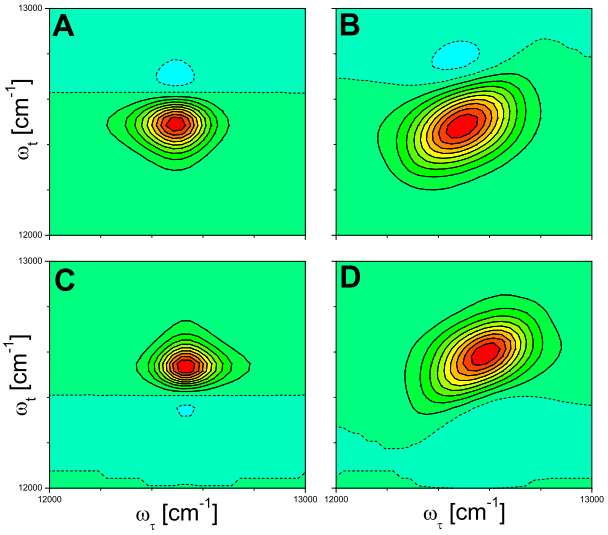

Figure 8: Two-dimensional correlation photon echo spectrum of a model pentamer. Subfigures: (A) radial configuration $\alpha = -\frac{\pi}{2}$, single realization; (B) radial configuration, averaged over disorder with $\Delta = 100$ cm^{-1}; (C) tangential configuration $\alpha = 0$, single realization; (D) tangential configuration, averaged over disorder with $\Delta = 100$ cm^{-1}. All site energies are $\epsilon = 12500$ cm^{-1} and $\Gamma = 1/300$ fs^{-1}. Contours as in Fig. 6.

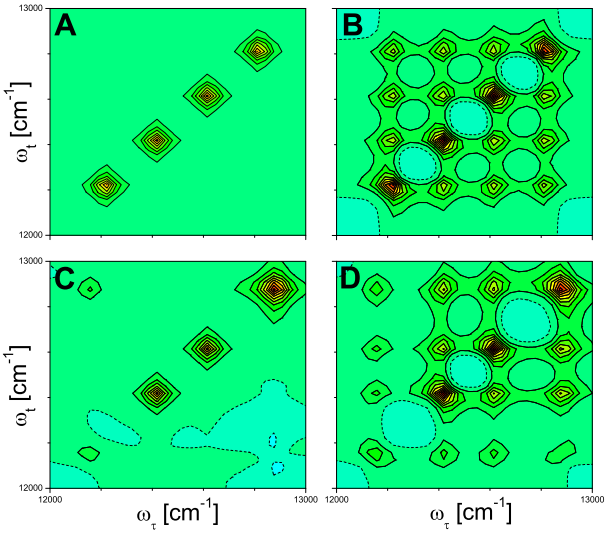

Figure 9: Demonstration of the additivity of 2D spectra. Subfigures: (A) Full 2D spectrum of a tetramer consisting of four uncoupled molecules, (B) the same calculation with ESA ignored, (C) Tetramer with only the lowest and highest energy molecules coupled to each other by $J = 100$ cm^{-1}, (D) The same case with ESA ignored. Site energies are $\epsilon = 12800$, 12600, 12400 and 12200 cm^{-1}, disorder width $\Delta = 0$ cm^{-1} and $\Gamma = 1/150$ fs^{-1}. Contours as in Fig. 6.

butions are correctly balanced. To this end we consider a hetero tetramer composed of four chromophores with distinct transition energies $\omega_1 = 12600$ cm^{-1},$\omega_2 = 12500$ cm^{-1},$\omega_3 = 12400$ cm^{-1} and $\omega_4 = 12300$ cm^{-1}. Fig. 9A presents a 2D spectrum of uncoupled tetramer. No crosspeaks and negative features appear and the spectrum is a sum of monomeric 2D spectra. When only ground state to one-exciton band transitions are considered and the aggregate ESA is ignored many crosspeaks appear in the 2D spectrum (Fig. 9B). All these crosspeaks are exactly canceled by the ESA contribution. When the lowest and highest energy monomers are coupled (here with $J = 200$cm^{-1}) the 2D spectrum becomes a sum of two independent monomers and a coupled dimer, Fig. 9C. Again, when the ESA contribution is removed, the redistribution of cross-peak amplitudes in ground state contribution can be clearly seen, but all cross-peaks involving the coupled dimer and the independent monomers are canceled out in Fig. 9D.

To calculate 2D spectrum of uncoupled monomers one can therefore simply calculate individual 2D spectra and sum them. However, the balance of ESA and the ground state contributions can be disrupted also by relaxation processes like FRET. Two monomers or two composed systems that are coupled weakly so that cross-peaks due to mutual interactions are too weak to be resolved, but nevertheless strong enough to enable energy transfer will show energy relaxation crosspeaks. This is e.g. the case of LH3 (see Ref. [14]). In case of LH3 one has to account for additional stimulated emission from the states populated by energy relaxation, and other similar processes. All this is included in the EM presented in this paper. Moreover, not all states involved in the theory have to be localized on individual monomers. We can equally divide the system into parts where excitonic interaction dominates, and start from excitons formed by this interaction. Mutual interaction of such blocks is then described by the theory presented here.

VII. CONCLUSIONS

In this paper we have derived EM for the reduced density matrix of a system of weakly coupled chromophores interacting with an environment. The weak excitonic coupling is treated in the second order perturbation theory and the environmental degrees of freedom are described within the second cumulant approximation, which for some type of systems provides an exact solution. We show that our equations are related to the Förster relaxation rates. In contrast to the usual Förster type equations, we provide a detailed prescription for the evolution of coherences. Thus, we are able to describe an effect of dynamic localization, where the bath destroys not only a wavepacket created in the complex by ultrafast excitation, but also the coherence established by the weak resonance coupling. By simulations of model systems in homogeneous limit we demonstrate that 2D spectroscopy

reveals the excitonic coupling by an offset of the excited state absorption, and that our local bases description of the systems dynamics is fully sufficient to account for this effect.

Acknowledgments

This work was partially supported by Czech Science Foundation (GACR) via grant nr. 205/10/0989 and by the Ministry of Education, Youth and Sports of the Czech republic via grant KONTAKT ME899 and research plan MSM0021620835. V.B. thanks to the European Physical Society for the support of his five months stay at Charles University in Prague in form of University Student Scholarship. L. V. is supported by the Scientific Council of Lithuania. The spectroscopic package NOSE is available under GNU Public License at http://www.sourceforge.net.

Appendix A: Cumulant expansion evaluation of the $M_{abcd}(t,\tau)$ matrix

Expanding each evolution operator $U_a(t)$ up to the second order,

$$U_a(t) \approx 1 - i\mathcal{H}_a(t) - \mathcal{G}_a^{(+)}(t), \tag{75}$$

$$U_a^{\dagger}(t) \approx 1 + i\mathcal{H}_a(t) - \mathcal{G}_a^{(-)}(t), \tag{76}$$

where

$$\mathcal{H}_a(t) = \frac{1}{\hbar}\int_0^t d\tau \Delta V_a(t), \tag{77}$$

$$\mathcal{G}_a^{(+)}(t) = \frac{1}{\hbar^2}\int_0^t d\tau \int_0^\tau d\tau' \Delta V(\tau)\Delta V(\tau'), \tag{78}$$

and

$$\mathcal{G}_a^{(-)}(t) = \frac{1}{\hbar^2}\int_0^t d\tau \int_0^\tau d\tau' \Delta V(\tau')\Delta V(\tau), \tag{79}$$

the auxiliary matrix M can be evaluated in the second order cummulant approximation. To that end we evaluate the following traces

$$Tr_Q\{\mathcal{H}_a(t)W_{eq}\} = 0, \tag{80}$$

$$Tr_Q\{\mathcal{G}_a^{(+)}(t)W_{eq}\} = g_a(t), \tag{81}$$

$$Tr_Q\{\mathcal{G}_a^{(-)}(t)W_{eq}\} = g_a^*(t), \tag{82}$$

$$Tr_Q\{\mathcal{H}_a(t)\mathcal{H}_b(\tau)W_{eq}\} = g_{ab}(t) - g_{ab}(t-\tau) + g_{ba}^*(\tau). \tag{83}$$

With these results we can evaluate the second order expansion of M

$$\begin{aligned} e^{-i\omega_{ab}t - i\omega_{cd}\tau} M_{abcd}(t,\tau) &= Tr_Q\Big\{\Big[1 + i\mathcal{H}_a(t) - \mathcal{G}_a^{(-)}(t)\Big] \\ &\times \Big[1 - i\mathcal{H}_b(t) - \mathcal{G}_b^{(+)}(t)\Big]\Big[1 + i\mathcal{H}_c(\tau) - \mathcal{G}_c^{(-)}(\tau)\Big] \\ &\times \Big[1 - i\mathcal{H}_d(\tau) - \mathcal{G}_d^{(+)}(\tau)\Big] W_{eq}\Big\} \\ &= Tr_Q\Big\{1 + \mathcal{H}_a(t)\mathcal{H}_b(t) - \mathcal{H}_a(t)\mathcal{H}_c(\tau) + \mathcal{H}_a(t)\mathcal{H}_d(\tau) \\ &+ \mathcal{H}_b(t)\mathcal{H}_c(\tau) - \mathcal{H}_b(t)\mathcal{H}_d(\tau) + \mathcal{H}_c(\tau)\mathcal{H}_d(\tau)\Big\} \\ &- Tr_Q\Big\{\mathcal{G}_a^{(-)}(t) + \mathcal{G}_b^{(+)}(t) + \mathcal{G}_c^{(-)}(\tau) + \mathcal{G}_d^{(+)}(\tau)\Big\}. \end{aligned} \tag{84}$$

Assuming that $g_{ab}(t) = 0$ if $a \neq b$, and taking into account that $a \neq b$ and $c \neq d$ in the M function we have

$$M_{abcd}(t,\tau) = e^{F_{abcd}(t,\tau) + i\omega_{ab}t + i\omega_{cd}\tau}, \tag{85}$$

where

$$\begin{aligned} F_{abcd}(t,\tau) &= -g_a^*(t) - g_b(t) - g_c^*(\tau) - g_d(\tau) \\ &- \delta_{ac}\left(g_a(t) - g_a(t-\tau) + g_a^*(\tau)\right) \\ &+ \delta_{ad}\left(g_a(t) - g_a(t-\tau) + g_a^*(\tau)\right) \\ &+ \delta_{bc}\left(g_b(t) - g_b(t-\tau) + g_b^*(\tau)\right) \\ &- \delta_{bd}\left(g_b(t) - g_b(t-\tau) + g_b^*(\tau)\right). \end{aligned} \tag{86}$$

Appendix B: Third order response functions

Here we present third order response functions for a three band system in state representation, using Einstein summation convention. The upper indices denote the bands so that g corresponds to the ground state band (for excitonic system only one state is assumed to be in the ground state band), e and f represent the one-exciton and two-exciton bands, respectively. Lower indices denote the states within the bands. In all equations below, index a represents a ground state index and consequently $a \equiv g$ and $\rho_a \equiv \rho_g$, where ρ_g is the initial population of the ground state.

$$R_{1g}(t_3,t_2,t_1) = \langle V_{ji}^{(ge)} V_{gh}^{(eg)} V_{ba}^{(eg)} V_{de}^{(ge)} \rangle$$

$$\times \mathcal{U}^{(eg)}_{ijfh}(t_3)\mathcal{U}^{(ee)}_{fgce}(t_2)\mathcal{U}^{(eg)}_{cdba}(t_1)\rho_a, \tag{87}$$

$$R_{1f}(t_3,t_2,t_1) = \langle V^{(fe)}_{ji} V^{(ef)}_{gh} V^{(eg)}_{ba} V^{(ge)}_{de}\rangle$$

$$\times \mathcal{U}^{(ef)}_{ijfh}(t_3)\mathcal{U}^{(ee)}_{fgce}(t_2)\mathcal{U}^{(eg)}_{cdba}(t_1)\rho_a, \tag{88}$$

$$R_{2g}(t_3,t_2,t_1) = \langle V^{(ge)}_{ji} V^{(eg)}_{gh} V^{(eg)}_{ec} V^{(ge)}_{ab}\rangle$$

$$\times \mathcal{U}^{(eg)}_{ijfh}(t_3)\mathcal{U}^{(ee)}_{fged}(t_2)\mathcal{U}^{(ge)}_{cdab}(t_1)\rho_a, \tag{89}$$

$$R_{2f}(t_3,t_2,t_1) = \langle V^{(fe)}_{ji} V^{(ef)}_{gh} V^{(eg)}_{ec} V^{(ge)}_{ab}\rangle$$

$$\times \mathcal{U}^{(ef)}_{ijfh}(t_3)\mathcal{U}^{(ee)}_{fged}(t_2)\mathcal{U}^{(ge)}_{cdab}(t_1)\rho_a, \tag{90}$$

$$R_{3g}(t_3,t_2,t_1) = \langle V^{(ge)}_{ji} V^{(eg)}_{hf} V^{(ge)}_{ab} V^{(eg)}_{de}\rangle$$

$$\times \mathcal{U}^{(eg)}_{ijhg}(t_3)\mathcal{U}^{(gg)}_{fgce}(t_2)\mathcal{U}^{(ge)}_{cdab}(t_1)\rho_a, \tag{91}$$

$$R_{3f}(t_3,t_2,t_1) = \langle V^{(fe)}_{ji} V^{(eg)}_{hf} V^{(ge)}_{ab} V^{(ef)}_{de}\rangle$$

$$\times \mathcal{U}^{(ef)}_{ijhg}(t_3)\mathcal{U}^{(gf)}_{fgce}(t_2)\mathcal{U}^{(ge)}_{cdab}(t_1)\rho_a, \tag{92}$$

$$R_{4g}(t_3,t_2,t_1) = \langle V^{(ge)}_{ji} V^{(eg)}_{hf} V^{(eg)}_{ec} V^{(eg)}_{ba}\rangle$$

$$\times \mathcal{U}^{(eg)}_{ijhg}(t_3)\mathcal{U}^{(gg)}_{fged}(t_2)\mathcal{U}^{(eg)}_{cdba}(t_1)\rho_a, \tag{93}$$

$$R_{4f}(t_3,t_2,t_1) = \langle V^{(ge)}_{ji} V^{(ef)}_{hf} V^{(fe)}_{ec} V^{(eg)}_{ba}\rangle$$

$$\times \mathcal{U}^{(eg)}_{ijhg}(t_3)\mathcal{U}^{(fg)}_{fged}(t_2)\mathcal{U}^{(eg)}_{cdba}(t_1)\rho_a. \tag{94}$$

The sign $\langle \ldots \rangle$ represents orientational averaging over possible orientations of a molecular system with respect to the polarization axis of the incident light. The orientational averaging is preformed for an isotropic distribution of orientations according to Refs. [36, 37].

Two-excitation Terms in Equation of Motion

In this appendix we present the details of $\mathcal{T}_2$ and $\mathcal{T}_3$ terms of the EM, Eq. (66), for two-excitation states.

$$\mathcal{T}_2 = \sum_{c=1}^{K}\Big[\sum_{\gamma=1}^{\sigma-1}\left[R^*_{ca\pi\gamma}(t) + R_{\gamma\pi ac}(t)\right]\rho_{c(\gamma\sigma)}(t)$$

$$+\sum_{\delta=\sigma+1}^{K}\left[R^*_{ca\pi\delta}(t) + R_{\delta\pi ac}(t)\right]\rho_{c(\sigma\delta)}(t)$$

$$+\sum_{\delta=\pi+1}^{K}\left[R^*_{ca\sigma\delta}(t) + R_{\delta\sigma ac}(t)\right]\rho_{c(\pi\delta)}(t)$$

$$+\sum_{\gamma=1}^{\pi-1}\left[R^*_{ca\sigma\gamma}(t) + R_{\gamma\sigma ac}(t)\right]\rho_{c(\gamma\pi)}(t)\Big]. \tag{95}$$

$$\mathcal{T}_3 = 2\sum_{\alpha=1}^{K}\sum_{\beta=\alpha+1}^{K}\Big(R^*_{\pi\beta\sigma\alpha}(t) + R^*_{\sigma\alpha\pi\beta}(t)$$

$$+R^*_{\pi\alpha\sigma\beta}(t) + R^*_{\sigma\beta\pi\alpha}(t)\Big)\bar{\rho}_{a(\alpha\beta)}(t)$$

$$+\sum_{\beta=\sigma+1}^{K}\sum_{\delta=\sigma+1}^{K}R^*_{\pi\delta\delta\beta}(t)\bar{\rho}_{a(\sigma\beta)}(t)$$

$$+\sum_{\alpha=1}^{\sigma-1}\sum_{\delta=\sigma+1}^{K}R^*_{\pi\delta\delta\alpha}(t)\bar{\rho}_{a(\alpha\sigma)}(t)$$

$$+\sum_{\beta=\pi+1}^{K}\sum_{\gamma=1}^{\pi-1}R^*_{\sigma\gamma\gamma\beta}(t)\bar{\rho}_{a(\pi\beta)}(t)$$

$$+\sum_{\alpha=1}^{\pi-1}\sum_{\gamma=1}^{\pi-1}R^*_{\sigma\gamma\gamma\alpha}(t)\bar{\rho}_{a(\alpha\pi)}(t)$$

$$+\sum_{\alpha=1}^{\sigma-1}\sum_{\gamma=1}^{\sigma-1}R^*_{\pi\gamma\gamma\alpha}(t)\bar{\rho}_{a(\alpha\sigma)}(t)$$

$$+\sum_{\beta=\sigma+1}^{K}\sum_{\gamma=1}^{\sigma-1}R^*_{\pi\gamma\gamma\beta}(t)\bar{\rho}_{a(\sigma\beta)}(t)$$

$$+\sum_{\delta=\pi+1}^{K}\sum_{\beta=\pi+1}^{K}R^*_{\sigma\delta\delta\beta}(t)\bar{\rho}_{a(\pi\beta)}(t)$$

$$+\sum_{\delta=\pi+1}^{N}\sum_{\alpha=1}^{\pi-1}R^*_{\sigma\delta\delta\alpha}(t)\bar{\rho}_{a(\alpha\pi)}(t). \tag{96}$$

[1] V. M. Agranovich and M. D. Galanin, *Excitation energy transfer in condensed matter* (North-Holland, Amsterdam, 1982).

[2] M. Pope and C. E. Swenberg, *Electronic processes in organic crystals*, 2 ed. (Oxford University Press, New York, 1999).

[3] H. van Amerongen, L. Valkunas, and R. van Grondelle, *Photosynthetic Excitons* (World Scientific, Singapore, 2000).

[4] *Primary Excitations in Conjugated Polymers: Molecular Exciton versus Semiconductor Band Model*, edited by N. S. Sariciftci (World Scientific, Singapore, 1997).

[5] E. A. Silinsh and V. Čápek, *Organic Molecular Crystals* (AIP Press, New York, 1994).

[6] R. E. Blankenship, *Molecular Mechanisms of Photosynthesis* (Blackwell Science, Oxford, 2002).

[7] Y. C. Cheng and R. J. Silbey, Phys. Rev. Lett. **96**, 028103 (2006).

[8] T. Mančal and L. Valkunas, Chem. Phys. Lett **432**, 301 (2006).

[9] G. S. Engel, T. R. Calhoun, E. L. Read, T. K. Ahn, T. Mančal, Y.-C. Cheng, R. E. Blankenship, and G. R. Fleming, Nature **446**, 782 (2007).

[10] H. Lee, Y.-C. Cheng, and G. R. Fleming, Science **316**, 1462 (2007).

[11] E. Collini and G. D. Scholes, Science **323**, 369 (2009).

[12] G. Panitchayangkoon, D. Hayes, K. A. Fransted, J. R. Caram, E. Harel, J. Wen, R. E. Blankenship, and G. S. Engel, (2010), arXiv:1001.5108v1 [physics.bio-ph].

[13] Y.-C. Cheng and G. R. Fleming, Annu. Rev. Phys. Chem. **60**, 241 (2009).

[14] D. Zigmantas, E. L. Read, T. Mančal, T. Brixner, A. T. Gardiner, R. J. Cogdell, and G. R. Fleming, P. Natl. Acad. Sci. USA **103**, 12672 (2006).

[15] J. Adolphs and T. Renger, Biophys. J. **91**, 2778 (2006).

[16] M. Lax, J. Chem. Phys. **20**, 1752 (1952).

[17] P. W. Anderson and P. R. Weiss, Rev. Mod. Phys. **24**, 269 (1953).

[18] R. Kubo, in *Fluctuation, relaxation and resonance in magnetic systems*, edited by D. ter Haar (Oliver and Boyd, Edinburgh, 1962).

[19] Y. Georgievskii, C.-P. Hsu, and R. A. Marcus, J. Chem. Phys. **110**, 5307 (1999).

[20] S. Mukamel, *Principles of Nonlinear Spectroscopy* (Oxford University Press, Oxford, 1995).

[21] T. Ha and J. Xu, Phys. Rev. Lett. **90**, 223002 (2003).

[22] E. A. Lipman, B. Schuler, O. Bakajin, and W. A. Eaton, Science **301**, 1233 (2003).

[23] G. McDermott, S. M. Prince, A. A. Freer, A. M. Hawthornthwaite-Lawless, M. Z. Papiz, R. J. Cogdell, and N. W. Isaacs, Nature **374**, 517 (1995).

[24] J. Koepke, X. C. Hu, C. Muenke, K. Schulten, and H. Michel, Structure **4**, 581 (1995).

[25] L. Valkunas, J. Janusonis, D. Rutkauskas, and R. van Grondelle, J. Luminesc. **127**, 269 (2007).

[26] J. Janusonis, L. Valkunas, D. Rutkauskas, and R. van Grondelle, Biophys. J. **94**, 1348 (2008).

[27] O. Zerlauskiene, G. Trinkunas, A. Gall, B. Robert, V. Urboniene, and L. Valkunas, J. Phys. Chem. B **112**, 15883 (2008).

[28] A. M. van Oijen, M. Katelaars, J. Kohler, T. Aartsma, and J. Schmidt, Chem. Phys. **247**, 53 (1999).

[29] O. Linden and V. May, Physica A **254**, 411 (1998).

[30] V. May and O. Kühn, *Charge and Energy Transfer Dynamics in Molecular Systems* (Wiley-VCH, Berlin, 2000).

[31] W. M. Zhang, T. Meier, V. Chernyak, and S. Mukamel, J. Chem. Phys. **108**, 7763 (1998).

[32] M. Yang and G. R. Fleming, Chem. Phys. **275**, 355 (2002).

[33] T. Brixner, T. Mančal, I. V. Stiopkin, and G. R. Fleming, J. Chem. Phys. **121**, 4221 (2004).

[34] NOSE package, `http://nose-project.sourceforge.net`.

[35] E. L. Read, G. S. Schlau-Cohen, G. S. Engel, J. Wen, R. E. Blankenship, and G. R. Fleming, J. Phys. Chem. B **113**, 6495 (2009).

[36] R. Hochstrasser, Chem. Phys. **266**, 273 (2001).

[37] J. Dreyer, A. M. Moran, and S. Mukamel, Bull. Korean Chem. Soc. **24**, 1091 (2003).